HHS Public Access

Author manuscript

Arterioscler Thromb Vasc Biol. Author manuscript; available in PMC 2024 April 10.

Published in final edited form as:

Arterioscler Thromb Vasc Biol. 2023 July ; 43(7): e279–e290. doi:10.1161/ATVBAHA.123.319332.

Latent Coronary Plaque Morphology From Computed Tomography Angiography, Molecular Disease Activity on Positron Emission Tomography, and Clinical Outcomes

Jacek Kwiecinski[*],

Márton Kolossváry[*],

Evangelos Tzolos,

Mohammed N. Meah,

Philip D. Adamson,

Nikhil V. Joshi,

Michelle C. Williams,

Edwin J.R. van Beek,

Daniel S. Berman,

Pál Maurovich-Horvat,

David E. Newby,

Marc R. Dweck,

Damini Dey,

Piotr J. Slomka

Departments of Medicine (Artificial Intelligence in Medicine), Imaging, and Biomedical Sciences, Cedars-Sinai Medical Center, Los Angeles, CA (J.K., E.T., D.S.B., D.D., P.J.S.). Department of Interventional Cardiology and Angiology, Institute of Cardiology, Warsaw, Poland (J.K.). Gottsegen National Cardiovascular Center, Budapest, Hungary (M.K.). Physiological Controls Research Center, University Research and Innovation Center, Óbuda University, Budapest, Hungary (M.K.). BHF Centre for Cardiovascular Science (E.T., M.N.M., M.C.W., E.J.R.v.B., D.E.N., M.R.B.) and Edinburgh Imaging, Queens Medical Research Institute (E.J.R.v.B.), University of Edinburgh, United Kingdom. Christchurch Heart Institute, University of Otago, Christchurch, New Zealand (P.D.A.). Bristol Heart Institute, University of Bristol, United Kingdom (N.V.J.). MTA-SE Cardiovascular Imaging Research Group, Department of Radiology, Medical Imaging Centre, Semmelweis University, Budapest, Hungary (P.M.-H.).

Abstract

Correspondence to: Piotr J. Slomka, PhD, Cedars-Sinai Medical Center, 8700 Beverly Blvd, Metro 203, Los Angeles, CA 90048. piotr.slomka@cshs.org.

[*]J. Kwiecinski and M. Kolossváry contributed equally.

Disclosures None.

Supplemental Material

Supplemental Material is available at https://www.ahajournals.org/doi/suppl/10.1161/ATVBAHA.123.319332.

For Sources of Funding and Disclosures, see page e289.

BACKGROUND: Assessments of coronary disease activity with ^{18}F-sodium fluoride positron emission tomography and radiomics-based precision coronary plaque phenotyping derived from coronary computed tomography angiography may enhance risk stratification in patients with coronary artery disease. We sought to investigate whether the prognostic information provided by these 2 approaches is complementary in the prediction of myocardial infarction.

METHODS: Patients with known coronary artery disease underwent coronary ^{18}F-sodium fluoride positron emission tomography and coronary computed tomography angiography on a hybrid positron emission tomography/computed tomography scanner. Coronary ^{18}F-NaF uptake was determined by the coronary microcalcification activity. We performed quantitative plaque analysis of coronary computed tomography angiography datasets and extracted 1103 radiomic features for each plaque. Using weighted correlation network analysis, we derived latent morphological features of coronary lesions which were aggregated to patient-level radiomics nomograms to predict myocardial infarction.

RESULTS: Among 260 patients with established coronary artery disease (age, 65±9 years; 83% men), 179 (69%) participants showed increased coronary ^{18}F-NaF activity (coronary microcalcification activity>0). Over 53 (40–59) months of follow-up, 18 patients had a myocardial infarction. Using weighted correlation network analysis, we derived 15 distinct eigen radiomic features representing latent morphological coronary plaque patterns in an unsupervised fashion. Following adjustments for calcified, noncalcified, and low-density noncalcified plaque volumes and ^{18}F-NaF coronary microcalcification activity, 4 radiomic features remained independent predictors of myocardial infarction (hazard ratio, 1.46 [95% CI, 1.03–2.08]; P=0.03; hazard ratio, 1.62 [95% CI, 1.04–2.54]; P=0.02; hazard ratio, 1.49 [95% CI, 1.07–2.06]; P=0.01; and hazard ratio, 1.50 (95% CI, 1.05–2.13); P=0.02).

CONCLUSIONS: In patients with established coronary artery disease, latent coronary plaque morphological features, quantitative plaque volumes, and disease activity on ^{18}F-sodium fluoride positron emission tomography are additive predictors of myocardial infarction.

GRAPHIC ABSTRACT:

A graphic abstract is available for this article.

Keywords

angiography; atherosclerosis; coronary artery disease; positron emission tomography; radiomics; tomography

---

Advanced cardiac imaging is a promising tool to enhance the risk stratification of patients with coronary artery disease (CAD). Through the identification of coronary plaque activity, 18F-sodium fluoride positron emission tomography (18F-NaF PET) can identify culprit plaques in patients with acute myocardial infarction and predict disease progression and future adverse events in subjects with stable CAD.[1–4] In addition, volumetric plaque analysis of coronary computed tomography angiography (CCTA) is an independent predictor of adverse cardiac events and complements PET-based plaque activity assessments.[3,5–7] Beyond plaque volumes, CCTA can also be used for precision phenotyping of CAD using radiomics.[5] By identifying latent plaque morphological features that are not captured

by standard CCTA analysis, radiomics enables a more detailed description of CAD phenotypes.[8] Prior reports have shown that CCTA radiomic analysis detects vulnerable plaques in patients with stable disease as validated by invasive and histological reference standards.[9,10]

Information regarding disease activity (assessed by ^{18}F-NaF PET) and plaque phenotypes (assessed by CCTA) can be obtained in a single imaging session using a hybrid PET/CT scanner. However, the complex interplay between molecular disease activity and latent plaque morphology is poorly understood. Furthermore, whether this information is complementary in predicting adverse events remains to be clarified. Therefore, we aimed to evaluate the associations between coronary plaque activity on PET and latent radiomic plaque morphology as assessed by CCTA radiomics and to investigate whether employing both these approaches further enhances risk stratification of patients with established disease.

METHODS

Study Population

The data underlying this article were provided by Cedars-Sinai Medical Center and The University of Edinburgh. Data can be shared on request to the corresponding author with permission from the contributing sites. We performed a post hoc analysis of prospective studies where patients underwent hybrid coronary ^{18}F-NaF PET and CCTA (https://www.clinicaltrials.gov; Unique identifiers: NCT01749254, NCT02110303, NCT02607748).[2,11,12] All patients had established CAD (with a history of either myocardial infarction or coronary revascularization) and underwent a comprehensive baseline clinical assessment including invasive coronary angiography and evaluation of their cardiovascular risk factor profile using the SMART (Secondary Manifestations of Arterial Disease) risk score.[13] In the current analysis, we excluded patients who had coronary stents within all coronary segments with atherosclerotic lesions because extraction of radiomic plaque features is not possible in this circumstance.[1] Studies were conducted with the approval of the local research ethics committee, in accordance with the Declaration of Helsinki, and written informed consent was obtained from each participant. We have provided a STROBE (Strengthening the Reporting of Observational Studies in Epidemiology) checklist in the Supplementary Material.

Imaging

Patients underwent ^{18}F-NaF PET on hybrid PET/CT scanners (128-slice Biograph mCT, Siemens Medical Systems; or Discovery 710, GE Healthcare) 60 minutes after intravenous administration of ^{18}F-NaF (250 MBq). During a single imaging session, we acquired a noncontrast CT attenuation correction scan followed by a 30-min PET scan in list mode, a low-dose noncontrast ECG-gated CT for calculation of the coronary calcium score, and an ECG-gated CCTA, which was obtained in mid-diastole and end-expiration without repositioning the patient. The ECG-gated PET list-mode dataset was reconstructed using harmonized protocols as described previously.[14]

^{18}F-NaF Uptake Quantification From PET

Image analysis was performed using FusionQuant following motion correction (Cedars-Sinai Medical Center).[15] In the first step, anatomic coronary artery data was extracted from coronary CT angiography by applying a vessel tracking algorithm based on Bayesian maximal paths (Autoplaque version 2.5). Second, a diffeomorphic mass-preserving image registration algorithm was used to align the 4 gates of PET data to the end-diastolic gate (FusionQuant Software, Cedars-Sinai Medical Center, Los Angeles). After motion correction, the 4 gates were summed together to build a motion-free image containing counts from the entire PET acquisition.[16]

We quantified 18F-NaF uptake activity across the entire coronary vasculature at the per-plaque, per-vessel, and per-patient level using the recently described coronary microcalcification activity (CMA).[17,18] Within automatically extracted whole-vessel tubular and tortuous 3-dimensional volumes of interest derived from the CCTA datasets, we measured CMA representing the overall disease activity in the vessel based on both the volume and intensity of ^{18}F-NaF PET activity. CMA was defined as the integrated activity in standardized uptake values units exceeding the corrected background blood pool mean standardized uptake values plus 2 standard deviations (right atrium activity). The per-patient CMA was defined as the sum of the per-vessel CMA values. A CMA>0 was regarded as positive and CMA=0 was considered as no ^{18}F-NaF uptake.

CT Analysis

The coronary artery calcium score was measured in Agatston units using clinical software (NetraMD, SCImage) on noncontrast CT scans. The presence, extent, and severity of CAD were evaluated on CCTA angiography by defining the segment involvement score and the number of vessels with >50% luminal stenosis.[19] Multivessel CAD was defined as at least 2 major epicardial vessels with any combination of either >50% stenosis or previous revascularization.

We performed quantitative plaque analysis of all nonstented coronary segments with a lumen diameter >2 mm using semiautomated software (Autoplaque, version 2.5, Cedars-Sinai Medical Center).[6,7] Proximal and distal limits of lesions were manually marked by an experienced reader after examination of CCTA images in multiplanar format. Subsequent plaque quantification was fully automated using adaptive scan-specific thresholds. Total, calcified, noncalcified, and low-attenuation plaque volumes were calculated.[6,7]

Extraction of Latent Plaque Morphological Features

All voxels defined as plaque by the semiautomated software (Autoplaque version 2.5) were loaded into the open-source Radiomics Image Analysis (version 1.4.2, https://cran.r-project.org/web/packages/RIA/index.html) software package in the R environment. Overall, 1103 radiomic features were calculated on each segmented coronary plaque image.[10] We implemented a recently published framework based on weighted correlation network analysis for the unsupervised extraction of the latent morphological features.[20,21] In brief, first we calculated the interpair similarity of the radiomic features correcting for intrapatient clustering using linear mixed models (individuals may have multiple plaques), which

included a random intercept per patient. Next, using this similarity matrix, we calculated the hierarchical clustering dendrogram of radiomic features and used the dynamic tree-cut algorithm to identify the optimal number of feature clusters among our radiomic parameters.[22] We then calculated the first principal component of each cluster, as the features within each cluster are highly correlated with each other and therefore may be the representation of the same latent plaque morphology. These principal eigen radiomic features are named as colors similar to the conventions in other -omics analyses.[21,23]

Clinical Follow-Up

The primary end point of the study was fatal or nonfatal myocardial infarction. Outcome information was obtained from the local and national healthcare record systems that integrate primary and secondary healthcare records. Categorization of these outcomes was performed blinded to the coronary PET or other study data. Outcome data were collected in July 2021.

Statistical Analysis

We assessed the distribution of data with the Shapiro-Wilk test. Continuous variables are presented as means and standard deviations or medians and interquartile ranges (Q1–Q3) as appropriate, while categorical parameters are reported as frequencies and percentages.

First, to assess whether the derived eigen radiomic features are associated with different plaque volumes, we created a heatmap of the correlations between each eigen feature and the plaque volumes correcting for intrapatient clustering using linear mixed models and reordered according to hierarchical clustering. Then, to assess the association between latent plaque morphologies and PET activity, we conducted univariable, multivariable logistic regression, and linear regression models on a per-plaque level between each eigen radiomic feature and ^{18}F-NaF CMA correcting for calcified, noncalcified, and low-attenuation plaque volumes.

Next, we summarized plaque level eigen radiomic features to patient-level parameters by taking the average of the features per patient, each weighted by the corresponding plaque volume. We used these patient-level eigen radiomic feature values first to assess which risk factors are associated with which eigen radiomic feature by including clinical risk factors into a model to predict each eigen radiomic feature separately. Then we used them in univariable Cox proportional hazard models to assess their predictive power to identify individuals at risk of fatal or nonfatal myocardial infarction. Multivariable Cox proportional hazard models including ^{18}F-NaF CMA were adjusted for calcified, noncalcified, and low-attenuation noncalcified plaque volumes. As the eigen radiomic features are correlated with each other, we were unable to include all of them in the same model, therefore, to assess the importance of clinical parameters, CAD characteristics, plaque volumes, PET activity, and eigen radiomic features to predict the primary end point, we built a survival random forest machine learning model with 10 000 repeats. Using 1000 subsamples, we calculated the variable importance and 95% CIs of all parameters (Figure 1). To improve the statistical power data from males and females were combined.

All statistical calculations were performed in the R environment (v.4.1.3), using statistical packages lmerTest (v.3.1.3), weighted correlation network analysis (v.1.70.3), survival (v.3.3.1) and randomForestSRC (v.3.0.2) A 2-sided $P<0.05$ was regarded as significant.[22,24–27]

RESULTS

Patients

The study population comprised of 260 patients (83% men; mean age, 65±9 years). All participants had established CAD and 215 (83%) had a history of prior revascularization. The majority of patients presented with cardiovascular risk factors (hypertension, 59%; hyperlipidemia, 90%; tobacco use, 66%) and were already on secondary preventative therapies (statin: 89%; anti-platelet therapy: 92%; angiotensin-converting enzyme inhibitor or angiotensin receptor blockers: 70%; Table 1). On invasive angiography performed at 42 (23–69) days before baseline imaging, 65 (25%) individuals had single-vessel coronary artery disease, 173 (67%) had multivessel coronary artery disease, and 14 (5%) had significant left main stem involvement.

CT and ^{18}F-NaF PET

The median CT calcium score was 294 (75–775) Agatston units; 141 (54%) patients had a calcium score >400 Agatston units, and only 76 (29%) presented with a score <100 Agatston units. On CCTA, the overall median segment involvement score was 6 (4–7). The median total plaque volume was 1174 (737–1787) mm^3 and consisted largely of noncalcified plaque (1100 [665–1574] mm^3) with a substantial volume of low-attenuation plaque (86 [44–164] mm^3). Fifty-seven percent of the study population (n=148) had a low-attenuation plaque burden exceeding 4%.

We identified increased 18F-NaF activity in 179 (69%) patients (CMA>0). Across the entire cohort, the median CMA was 0.64 (0.0–2.53). At the individual coronary plaque level among a grand total of 1495 lesions, 313 (21%) demonstrated an increased ^{18}F-NaF activity (CMA>0). There was a moderate correlation between total plaque volumes and continuous CMA values (r=0.43, $P<0.001$). Similar to previous studies, although calcified plaque volumes were weakly associated with ^{18}F-NaF uptake (r=0.22, $P<0.001$), CMA had a moderate correlation with noncalcified plaque volumes (r=0.48, $P<0.001$) and a stronger correlation with low-attenuation plaque volumes (r=0.61, $P<0.001$).

Radiomics

Using the calculated 1103 radiomic features, we mapped the latent morphological pattern of the coronary plaques by first calculating the interpair similarity between each feature. A heatmap with the corresponding hierarchical dendrogram is presented in Figure 2A. Using the dynamic tree-cut algorithm, we identified 15 feature clusters. Plotting these using a multidimensional scaling plot, we found the feature clusters to be separated in latent space, indicating that the clusters represent different information regarding the morphology of the lesions (Figure 2B). We then calculated the corresponding eigen radiomic feature for each cluster, resulting in 15 latent morphological features which we used for further analysis.

Association Between Plaque Volumes and Latent Plaque Morphological Features

To assess whether the derived eigen radiomic features represent information above and beyond plaque volumes, we calculated the correlation between the eigen radiomic features and the plaque components. Hierarchical clustering of the features showed that many features had low correlation with any of the plaque volumes (Yellow, Turquoise, etc), while other features were associated with noncalcified and low-attenuation noncalcified plaque volumes (Salmon; Figure 3). Furthermore, the heatmap indicated that some eigen radiomic features are correlated with each other, indicating that these features may organize into higher order feature meta-clusters similar to other biological concepts such as the proteome.

Interplay Between Plaque Radiomics and ^{18}F-NaF Uptake

At the individual coronary plaque level of the 15 eigen radiomic features, 9 were associated with CMA values on univariable linear regression analysis. Importantly, 4 eigen features remained independently associated with CMA in multivariable analysis following adjustments for calcified, noncalcified, and low-attenuation plaque volumes (Table 2). The remaining 6 plaque morphological features were not associated with PET activity. When ^{18}F-NaF was considered as a binary variable, 12 radiomic clusters were associated with PET positivity. Again, following adjustments for plaque volumes, these associations persisted with 11 radiomics clusters (Table 3). All of the radiomic features which were associated with ^{18}F-NaF CMA on linear regression were also related to the presence of ^{18}F-NaF activity on logistic regression (Table 3).

Association Between Eigen Radiomic Features and Risk Factors

To assess which risk factors are associated with specific plaque morphologies, we entered patient characteristics into a regression model to predict the patient-level eigen radiomic values. Several of the eigen radiomic features were associated with diabetes (Table 4).

Outcome Analyses

Over the 53 (40–59) months of follow-up, 18 subjects experienced a fatal (n=2) or nonfatal (n=16) myocardial infarction. On univariate Cox modeling, 7 of the eigen radiomic features, low-attenuation plaque volume, and CMA emerged as predictors of myocardial infarction. Among these 7 eigen radiomics features, Salmon, Brown, Pink, and Purple were associated with CMA, whereas Yellow, Red, and Cyan were not. Following adjustments for calcified, noncalcified, and low-density noncalcified plaque volumes and ^{18}F-NaF CMA, 4 latent eigen radiomic features remained independent predictors of myocardial infarction. Among these, Salmon, Brown, and Pink were associated with ^{18}F-NaF CMA, but Yellow was not (Table 5).

We assessed the variable importance of clinical parameters, CAD characteristics, plaque volumes, PET activity, and eigen radiomic features to predict the primary end point using random forest survival machine learning models (Figure 4). We found that the most important feature to predict adverse outcomes considering all parameters was overall CMA activity. None of the clinical or CAD characteristics influenced the prediction of the primary outcome. Furthermore, among plaque volumes, only low-attenuation plaque had prognostic value. Our results show that beyond PET activity, Purple, Red, Cyan,

Pink, Brown, Yellow, and Magenta eigen radiomic features had a role in predicting fatal or nonfatal myocardial infarction. Among these radiomic features, Purple, Pink, Brown, and Magenta were associated with PET activity while Red, Cyan, and Yellow were not associated with ^{18}F-NaF CMA (Figures 1 and 4).

DISCUSSION

In our multimodality imaging study, we characterized the complex interplay between coronary plaque composition, morphology, and activity in patients with established CAD. We showed that radiomic analysis of CCTA images allows the identification of latent morphological features, some of which are correlated with PET activity, and some of which are not. We demonstrated that while among variables assessed in our study CMA from PET is the strongest predictor of myocardial infarction, both volumetric and radiomic CT features also have prognostic implications. Importantly, the radiomics analysis of coronary plaques provided additive predictive value for myocardial infarction above and beyond both plaque volumes and ^{18}F-NaF CMA.

Over the past decade, quantitative plaque analysis has substantially improved risk stratification beyond conventional qualitative assessments.[6,7] These quantitative plaque measures complement disease activity assessments with PET so that the combination of both provides the most robust prediction of myocardial infarctions.[3] However, CT datasets contain additional embedded information that is unrecognized and unused during conventional clinical interpretation. This latent information can be extracted using radiomics: the process of deriving quantitative metrics from medical images to create big-data datasets, within which every lesion is characterized by hundreds of different parameters.[20] By considering the complex spatial relationship between voxels, radiomics provides an objective, automated, and data-driven description of plaque morphology. In patients undergoing CCTA, radiomics outperformed conventional qualitative and quantitative analysis in identifying vulnerable plaques as detected on invasive coronary imaging.[9] Moreover, in patients presenting with acute myocardial infarction, radiomic features can provide incremental value for distinguishing culprit lesions beyond state-of-the-art CCTA-based plaque assessments.[5] A particularly promising application of coronary plaque radiomics analysis is the ability for longitudinal assessment of changes in lesion structure above and beyond changes in plaque volumes, which may allow better monitoring of lesion characteristics following therapeutical interventions.[21]

Until recently, one of the major limitations of radiomics was the abundant number of variables that are routinely extracted. In most prior analyses, each and every feature was analyzed independently. However, this results in hundreds and thousands of statistical tests being conducted, which requires stringent corrections for false discoveries and type 1 error. Furthermore, individual radiomic features can be nonreproducible and redundant.[28,29] In the current study, we employed a recently described workflow that allowed the identification of a small number of robust and reproducible eigen radiomic features, which are summary variables of the underlying latent morphological characteristics.[21] Utilizing principal component analysis, we reduced the number of morphological features from 1103 to 15 robust eigen radiomic features, allowing for conventional statistical analysis. This

approach facilitated identifying key latent morphological features, which acted as predictors of adverse outcomes during follow-up.

^{18}F-NaF uptake reflects calcification activity and is associated with future disease progression and adverse outcomes across a wide range of cardiovascular conditions including aortic stenosis, mitral annular calcification, abdominal aortic aneurysm, and bioprosthetic valve degeneration.[30–37] If CT radiomic analysis could provide similar risk stratification to ^{18}F-NaF PET uptake, then this would greatly benefit patients due to improved availability, reduction in radiation exposure, and better cost-effectiveness. This notion is particularly compelling in view of the predictive value of ^{18}F-NaF coronary uptake in patients with established CAD where none of the existing risk scores provided robust risk stratification.[1] To explore the interplay between plaque radiomics and PET activity, we leveraged our prior cohort of patients with established CAD, in whom subjects with a high ^{18}F-NaF uptake had an 8-fold increase in the risk of myocardial infarction over 4 years of follow-up.[1] In our current analysis, 4 out of 15 radiomic clusters acted as independent predictors of adverse outcomes following adjustments for plaque volumes and coronary ^{18}F-NaF uptake. These included radiomic features which were not associated with ^{18}F-NaF uptake. This observation suggests that despite the strong associations between ^{18}F-NaF and the majority of latent radiomic morphological plaque features, the information provided by these 2 modalities is complementary. This is shown in our machine learning analysis where the most important feature to predict adverse outcomes was the ^{18}F-NaF CMA. However, while risk factors and clinical CAD markers did not contribute to the predictions, low-attenuation noncalcified plaque and several of the eigen radiomics features did. Of the 7 eigen radiomics features which were associated with later outcomes, 4 were associated with ^{18}F-NaF CMA, while 3 were not. These data suggest that radiomics might facilitate the identification of patients who experience myocardial infarction during follow-up, yet at baseline imaging present without ^{18}F-NaF coronary uptake and unfavorable plaque volumes on quantitative plaque analysis. Although in our study population all patients who had adverse events had a CMA>0 on PET, in the future the aforementioned hypothesis could be further tested.

Clinically, CCTA radiomics and ^{18}F-NaF coronary PET could be deployed in a staged approach. A prior CTA and subsequent PET-only acquisition protocol lends itself to a practical clinical workflow, with the initial CTA providing a basis for selection of patients for the coronary PET study.[14] Ultimately, these advanced atherosclerotic plaque assessments could serve for the optimal allocation of expensive medication including PCSK9 (proprotein convertase subtilisin/kexin type 9) or interleukin 1-beta inhibition to patients at the highest risk of adverse cardiovascular events.[38]

Limitations

Our study has several strengths and weaknesses. Although we analyzed data from 2 imaging centers which were acquired in the context of 3 independent prospective studies representing the largest cohort of patients with established coronary artery disease who have undergone ^{18}F-NaF PET to date, the study population remains modest in size. As a consequence, the number of events is limited. Furthermore, the generalizability of our findings needs to be

validated due to the limited variation in imaging hardware and software, and the potential bias of running several different models. Our findings, therefore, require confirmation in future studies. Fortunately, the PREFFIR study (Prediction of Recurrent Events With ^{18}F-Fluoride), in which patients with a recent myocardial infarction underwent ^{18}F-NaF coronary PET and are followed up for recurrent events, shall provide an opportunity to further explore the interplay between coronary plaque molecular activity and latent morphological features. To date, we lack data on the feasibility and potential insights that could be obtained from coronary PET radiomic analysis. Future studies should therefore address this important topic.

Conclusions

Radiomic analysis of CCTA images allows the identification of latent morphological phenotypes, of which some are highly correlated with the ^{18}F-NaF coronary activity while some are not. In patients with established CAD, latent coronary plaque radiomic features, along with quantitative plaque analysis measures and plaque activity on ^{18}F-NaF PET, are additive predictors of myocardial infarction.

Supplementary Material

Refer to Web version on PubMed Central for supplementary material.

Sources of Funding

This research was supported in part by grants R35HL161195 and R01HL133616 from the National Heart, Lung, and Blood Institute/National Institute of Health (NHLBI/NIH). The content is solely the responsibility of the authors and does not necessarily represent the official views of the National Institutes of Health. D.E. Newby (CH/09/002, RE/18/5/34216, RG/16/10/32375), M.R. Dweck (FS/14/78/31020), M.N. Meah (FS/19/46/34445), and M.C. Williams (FS/11/014, CH/09/002, FS/ICRF/20/26002) are supported by the British Heart Foundation. P.D. Adamson is supported by the Heart Foundation of New Zealand Senior Fellowship (1844). E. Tzolos was supported by a grant from Dr Miriam and Sheldon G. Adelson Medical Research Foundation. D.E. Newby is the recipient of a Wellcome Trust Senior Investigator Award (WT103782AIA) and M.R. Dweck of the Sir Jules Thorn Award for Biomedical Research Award (2015). E.J.R. van Beek is supported by SINAPSE (Scottish Imaging Network-A Platform of Scientific Excellence). N.V. Joshi is supported by the Medical Research Council through the MRC Clinical Academic Research Partnership grant (MR/T005459/1).

Nonstandard Abbreviations and Acronyms

^{18}F-NaF PET	^{18}F-sodium fluoride positron emission tomography
CAD	coronary artery disease
CCTA	coronary computed tomography angiography
CMA	coronary microcalcification activity
CT	computed tomography
PET	positron emission tomography
PREFFIR	Prediction of Recurrent Events With ^{18}F-Fluoride
SMART	Secondary Manifestations of Arterial Disease

REFERENCES

1. Kwiecinski J, Tzolos E, Adamson PD, Cadet S, Moss AJ, Joshi N, Williams MC, van Beek EJR, Dey D, Berman DS, et al. Coronary 18F-sodium fluoride uptake predicts outcomes in patients with coronary artery disease. J Am Coll Cardiol. 2020;75:3061–3074. doi: 10.1016/j.jacc.2020.04.046 [PubMed: 32553260]
2. Joshi NV, Vesey AT, Williams MC, Shah ASV, Calvert PA, Craighead FHM, Yeoh SE, Wallace W, Salter D, Fletcher AM, et al. 18F-fluoride positron emission tomography for identification of ruptured and high-risk coronary atherosclerotic plaques: a prospective clinical trial. Lancet. 2014;383:705–713. doi: 10.1016/S0140-6736(13)61754-7 [PubMed: 24224999]
3. Kwiecinski J, Tzolos E, Meah MN, Cadet S, Adamson PD, Grodecki K, Joshi NV, Moss AJ, Williams MC, van Beek EJR, et al. Machine-learning with 18F-sodium fluoride PET and quantitative plaque analysis on CT angiography for the future risk of myocardial infarction. J Nucl Med. 2022;63:158–165. doi: 10.2967/jnumed.121.262283 [PubMed: 33893193]
4. Kitagawa T, Yamamoto H, Nakamoto Y, Sasaki K, Toshimitsu S, Tatsugami F, Awai K, Hirokawa Y, Kihara Y. Predictive value of 18F-sodium fluoride positron emission tomography in detecting high-risk coronary artery disease in combination with computed tomography. J Am Heart Assoc. 2018;7:e010224. doi: 10.1161/JAHA.118.010224
5. Lin A, Kolossváry M, Cadet S, McElhinney P, Goeller M, Han D, Yuvaraj J, Nerlekar N, Slomka PJ, Marwan M, et al. Radiomics-based precision phenotyping identifies unstable coronary plaques from computed tomography angiography. JACC Cardiovasc Imaging. 2022;15:859–871. doi: 10.1016/j.jcmg.2021.11.016 [PubMed: 35512957]
6. Williams MC, Kwiecinski J, Doris M, McElhinney P, D'Souza MS, Cadet S, Adamson PD, Moss AJ, Alam S, Hunter A, et al. Low-attenuation noncalcified plaque on coronary computed tomography angiography predicts myocardial infarction: results from the multicenter SCOT-HEART trial (Scottish Computed Tomography of the HEART). Circulation. 2020;141:1452–1462. doi: 10.1161/CIRCULATIONAHA.119.044720 [PubMed: 32174130]
7. Lin A, Manral N, McElhinney P, Killekar A, Matsumoto H, Kwiecinski J, Pieszko K, Razipour A, Grodecki K, Park C, et al. K Deep learning from coronary computed tomography angiography for atherosclerotic plaque and stenosis quantification and cardiac risk prediction: an international multicentre study. Lancet Digit Health. 2022;4:e256256–e25e265. doi: 10.1016/s2589-7500(22)00022-x
8. Aerts HJWL. The potential of radiomic-based phenotyping in precision medicine: a review. JAMA Oncol. 2016;2:1636–1642. doi: 10.1001/jamaoncol.2016.2631 [PubMed: 27541161]
9. Kolossváry M, Park J, Bang JI, Zhang J, Lee JM, Paeng JC, Merkely B, Narula J, Kubo T, Akasaka T, et al. Identification of invasive and radionuclide imaging markers of coronary plaque vulnerability using radiomic analysis of coronary computed tomography angiography. Eur Heart J Cardiovasc Imaging. 2019;20:1250–1258. doi: 10.1093/ehjci/jez033 [PubMed: 30838375]
10. Kolossváry M, Karády J, Kikuchi Y, Ivanov A, Schlett CL, Lu MT, Foldyna B, Merkely B, Aerts HJ, Hoffmann U, et al. Radiomics versus visual and histogram-based assessment to identify atheromatous lesions at coronary CT angiography: an ex vivo study. Radiology. 2019;293:89–96. doi: 10.1148/radiol.2019190407 [PubMed: 31385755]
11. Moss AJ, Dweck MR, Doris MK, Andrews JPM, Bing R, Forsythe RO, Cartlidge TR, Pawade TA, Daghem M, Raftis JB, et al. Ticagrelor to reduce myocardial injury in patients with high-risk coronary artery plaque. JACC Cardiovasc Imaging. 2020;13:1549–1560. doi: 10.1016/j.jcmg.2019.05.023 [PubMed: 31422134]
12. Doris MK, Meah MN, Moss AJ, Andrews JPM, Bing R, Gillen R, Weir N, Syed M, Daghem M, Shah A, et al. Coronary 18F-fluoride uptake and progression of coronary artery calcification. Circ Cardiovasc Imaging. 2020;13:e011438. doi: 10.1161/CIRCIMAGING.120.011438
13. Dorresteijn JA, Visseren FL, Wassink AM, Gondrie MJ, Steyerberg EW, Ridker PM, Cook NR, van der Graaf Y; SMART Study Group. Development and validation of a prediction rule for recurrent vascular events based on a cohort study of patients with arterial disease: the SMART risk score. Heart. 2013;99:866–872. doi: 10.1136/heartjnl-2013-303640 [PubMed: 23574971]
14. Kwiecinski J, Adamson PD, Lassen ML, Doris MK, Moss AJ, Cadet S, Jansen MA, Dey D, Lee S-E, Yun M, et al. Feasibility of coronary 18F-sodium fluoride PET assessment with the utilization

of previously acquired CT angiography. Circ Cardiovasc Imaging. 2018;11:e008325. doi: 10.1161/CIRCIMAGING.118.008325

15. Massera D, Doris MK, Cadet S, Kwiecinski J, Pawade TA, Peeters FECM, Dey D, Newby DE, Dweck MR, Slomka PJ. Analytical quantification of aortic valve 18F-sodium fluoride PET uptake. J Nucl Cardiol. 2020;27:962–972. doi: 10.1007/s12350-018-01542-6 [PubMed: 30499069]
16. Lassen ML, Kwiecinski J, Dey D, Cadet S, Germano G, Berman DS, Adamson PD, Moss AJ, Dweck MR, Newby DE, et al. Triple-gated motion and blood pool clearance corrections improve reproducibility of coronary 18F-NaF PET. Eur J Nucl Med Mol Imaging. 2019;46:2610–2620. doi: 10.1007/s00259-019-04437-x [PubMed: 31385011]
17. Kwiecinski J, Cadet S, Daghem M, Lassen ML, Dey D, Dweck MR, Berman DS, Newby DE, Slomka PJ. Whole-vessel coronary 18F-sodium fluoride PET for assessment of the global coronary microcalcification burden. Eur J Nucl Med Mol Imaging. 2020;47:1736–1745. doi: 10.1007/s00259-019-04667-z [PubMed: 31897586]
18. Tzolos E, Kwiecinski J, Lassen ML, Cadet S, Adamson PD, Moss AJ, Joshi N, Williams MC, van Beek EJR, Dey D, et al. Observer repeatability and interscan reproducibility of 18F-sodium fluoride coronary microcalcification activity. J Nucl Cardiol. 2022;29:126–135. doi: 10.1007/s12350-020-02221-1 [PubMed: 32529531]
19. Leipsic J, Abbara S, Achenbach S, Cury R, Earls JP, Mancini GJ, Nieman K, Pontone G, Raff GL. SCCT guidelines for the interpretation and reporting of coronary CT angiography: a report of the Society of Cardiovascular Computed Tomography Guidelines Committee. J Cardiovasc Comput Tomogr. 2014;8:342–358. doi: 10.1016/j.jcct.2014.07.003 [PubMed: 25301040]
20. Kolossvary M 2021 RIA: Radiomics Image Analysis Toolbox for Grayscale Images. https://cran.r-project.org/web/packages/RIA/index.html
21. Kolossváry M, Bluemke DA, Fishman EK, Gerstenblith G, Celentano D, Mandler RN, Khalsa J, Bhatia S, Chen S, Lai S, et al. Temporal assessment of lesion morphology on radiological images beyond lesion volumes—a proof-of-principle study. Eur Radiol. 2022;32:8748–8760. doi: 10.1007/s00330-022-08894-1 [PubMed: 35648210]
22. Langfelder P, Horvath S. WGCNA: an R package for weighted correlation network analysis. BMC Bioinf. 2008;9:559. doi: 10.1186/1471-2105-9-559
23. Zhang B, Horvath S. A general framework for weighted gene co-expression network analysis. Stat Appl Genet Mol Biol. 2005;4:Article17. doi: 10.2202/1544-6115.1128
24. Kuznetsova A, Brockhoff PB, Christensen RHB. lmerTest package: tests in linear mixed effects models. J Stat Softw. 2017;82:1–26. doi: 10.18637/jss.v082.i13
25. Langfelder P, Horvath S. Fast R functions for robust correlations and hierarchical clustering. J Stat Softw. 2012;46:1–17. http://www.jstatsoft.org/v46/i11/ [PubMed: 22837731]
26. Therneau TM, Grambsch PM. Modeling Survival Data: Extending the Cox Model. Springer; 2000.
27. Ishwaran H, Kogalur UB, Blackstone EH, Lauer MS. Random survival forests. Ann Appl Statist. 2008;2:841–860. doi: 10.1214/08-AOAS169
28. Meyer M, Ronald J, Vernuccio F, Nelson RC, Ramirez-Giraldo JC, Solomon J, Patel BN, Samei E, Marin D. Reproducibility of CT radiomic features within the same patient: influence of radiation dose and CT reconstruction settings. Radiology. 2019;293:583–591. doi: 10.1148/radiol.2019190928 [PubMed: 31573400]
29. Berenguer R, Pastor-Juan MDR, Canales-Vázquez J, Castro-García M, Villas MV, Mansilla Legorburo F, Sabater S. Radiomics of CT features may Be nonreproducible and redundant: influence of CT acquisition parameters. Radiology. 2018;288:407–415. doi: 10.1148/radiol.2018172361 [PubMed: 29688159]
30. Tzolos E, Kwiecinski J, Berman D, Slomka P, Newby DE, Dweck MR. Latest advances in multimodality imaging of aortic stenosis. J Nucl Med. 2022;63:353–358. doi: 10.2967/jnumed.121.262304 [PubMed: 34887339]
31. Massera D, Trivieri MG, Andrews JP, Sartori S, Abgral R, Chapman AR, Jenkins WSA, Vesey AT, Doris MK, Pawade TA, et al. Disease activity in mitral annular calcification. Circ Cardiovasc Imaging. 2019;12:e008513. doi: 10.1161/CIRCIMAGING.118.008513
32. Forsythe RO, Dweck MR, McBride OMB, Vesey AT, Semple SI, Shah ASV, Adamson PD, Wallace WA, Kaczynski J, Ho W, et al. 18F-sodium fluoride uptake in abdominal

aortic aneurysms: the SoFIA3 study. J Am Coll Cardiol. 2018;71:513–523. doi: 10.1016/j.jacc.2017.11.053 [PubMed: 29406857]

33. Cartlidge TRG, Doris MK, Sellers SL, Pawade TA, White AC, Pessotto R, Kwiecinski J, Fletcher A, Alcaide C, Lucatelli C, et al. Detection and prediction of bioprosthetic aortic valve degeneration. J Am Coll Cardiol. 2019;73:1107–1119. doi: 10.1016/j.jacc.2018.12.056 [PubMed: 30871693]
34. Kwiecinski J, Tzolos E, Cartlidge TRG, Fletcher A, Doris MK, Bing R, Tarkin JM, Seidman MA, Gulsin GS, Cruden NL, et al. Native aortic valve disease progression and bioprosthetic valve degeneration in patients with transcatheter aortic valve implantation. Circulation. 2021;144:1396–1408. doi: 10.1161/CIRCULATIONAHA.121.056891 [PubMed: 34455857]
35. Irkle A, Vesey AT, Lewis DY, Skepper JN, Bird JLE, Dweck MR, Joshi FR, Gallagher FA, Warburton EA, Bennett MR, et al. Identifying active vascular microcalcification by (18)F-sodium fluoride positron emission tomography. Nat Commun. 2015;6:7495. doi: 10.1038/ncomms8495 [PubMed: 26151378]
36. Tzolos E, Dweck MR. 18F-sodium fluoride (18F-NaF) for imaging microcalcification activity in the cardiovascular system. Arterioscler Thromb Vasc Biol. 2020;40:1620–1626. doi: 10.1161/ATVBAHA.120.313785 [PubMed: 32375543]
37. Raggi P, Senior P, Shahbaz S, Kaul P, Hung R, Coulden R, Yeung R, Abele J. 18F-sodium fluoride imaging of coronary atherosclerosis in ambulatory patients with diabetes mellitus. Arterioscler Thromb Vasc Biol. 2019;39:276–284. doi: 10.1161/ATVBAHA.118.311711. Erratum in: Arterioscler Thromb Vasc Biol. 2019 Dec;39(12):e292 [PubMed: 30580559]
38. ClinicalTrials.gov. National Library of Medicine (U.S.). Effect of Evolocumab on Coronary Artery Plaque Volume and Composition by CCTA and Microcalcification by F18-NaF PET. 2018. Accessed March 4, 2023. https://ClinicalTrials.gov/show/NCT03689946.

Highlights

- In patients with established coronary artery disease plaque activity on ^{18}F-sodium fluoride positron emission tomography, composition on quantitative plaque analysis, and latent morphology assessed using radiomics on coronary computed tomography angiography are all predictors of myocardial infarction.
- Among variables assessed in our study, in patients with known coronary artery disease, plaque activity depicted with ^{18}F-sodium fluoride positron emission tomography is the dominant predictor of myocardial infarction.
- In patients with established coronary artery disease for optimal risk stratification, plaque activity, composition, and morphology should be considered jointly.

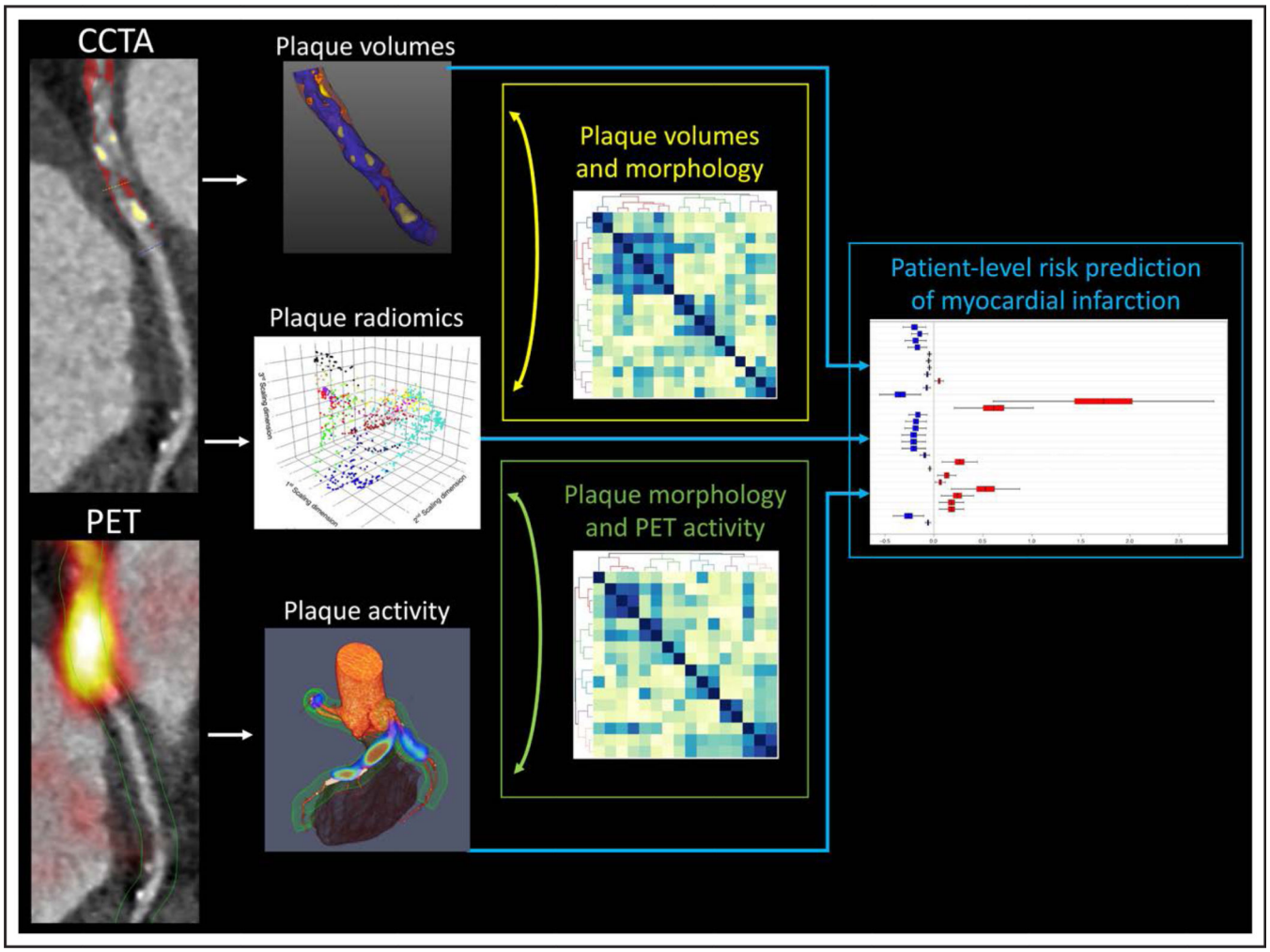

Figure 1. Prediction of myocardial infarction using disease activity imaging with 18F-sodium fluoride positron emission tomography (18F-NaF PET) and plaque radiomics and volumes imaging with coronary computed tomography angiography (CCTA).

In patients with established coronary artery disease assessments of plaque volumes, latent morphology, and activity are complementary predictors of myocardial infarction.

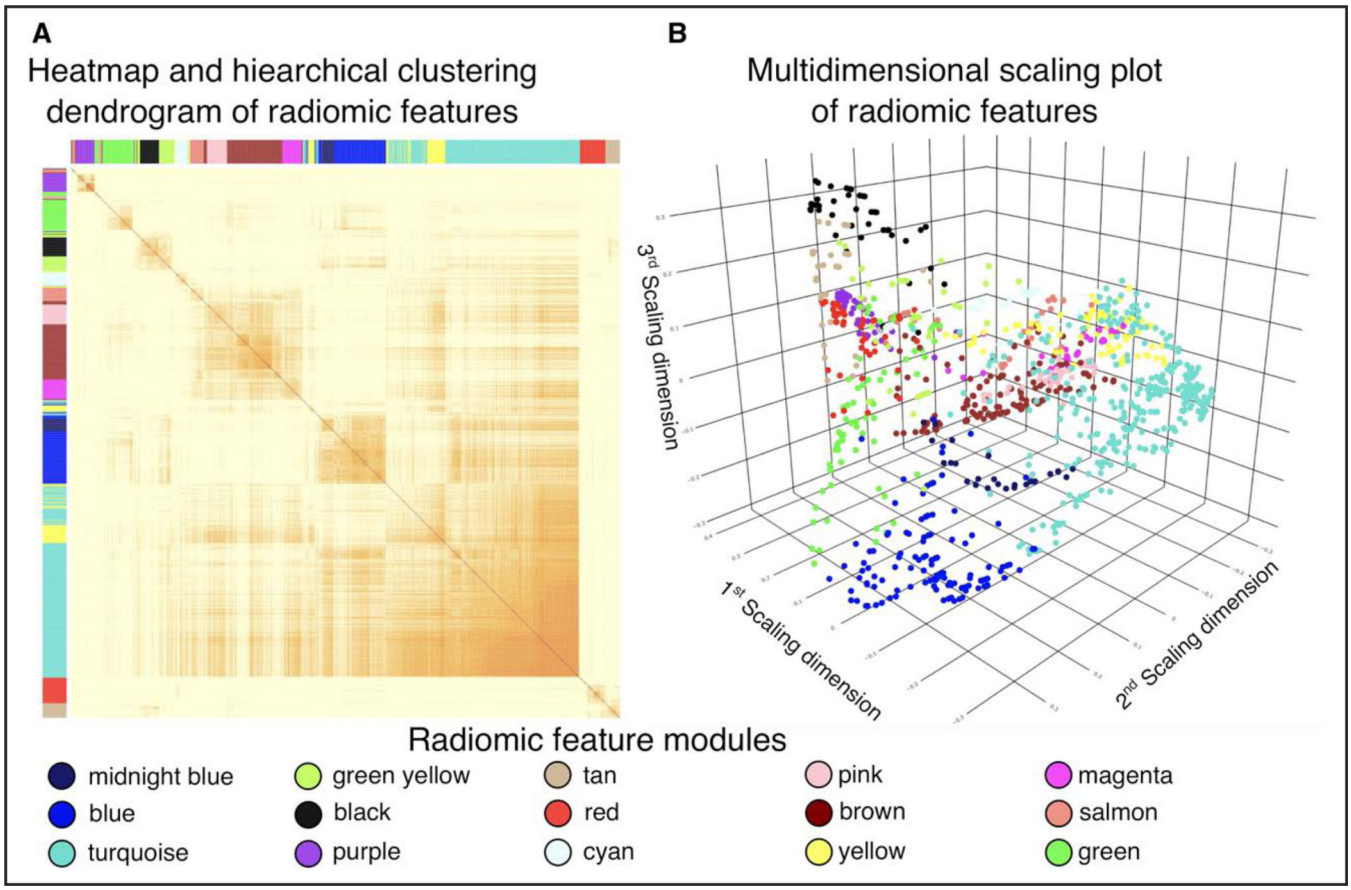

Figure 2. Visual representation of radiomic feature modules.

A, The interpair correlation values between each radiomic feature corrected for intrapatient clustering using linear mixed models. Rows and columns are reordered based on hierarchical clustering. The resulting radiomic feature models are shown using different colors. **B**, Multidimensional scaling plot of the radiomic features, where each point represents a radiomic parameter which is situated in the latent space according to the similarity to other parameters and is colored based on the radiomic module assignment.

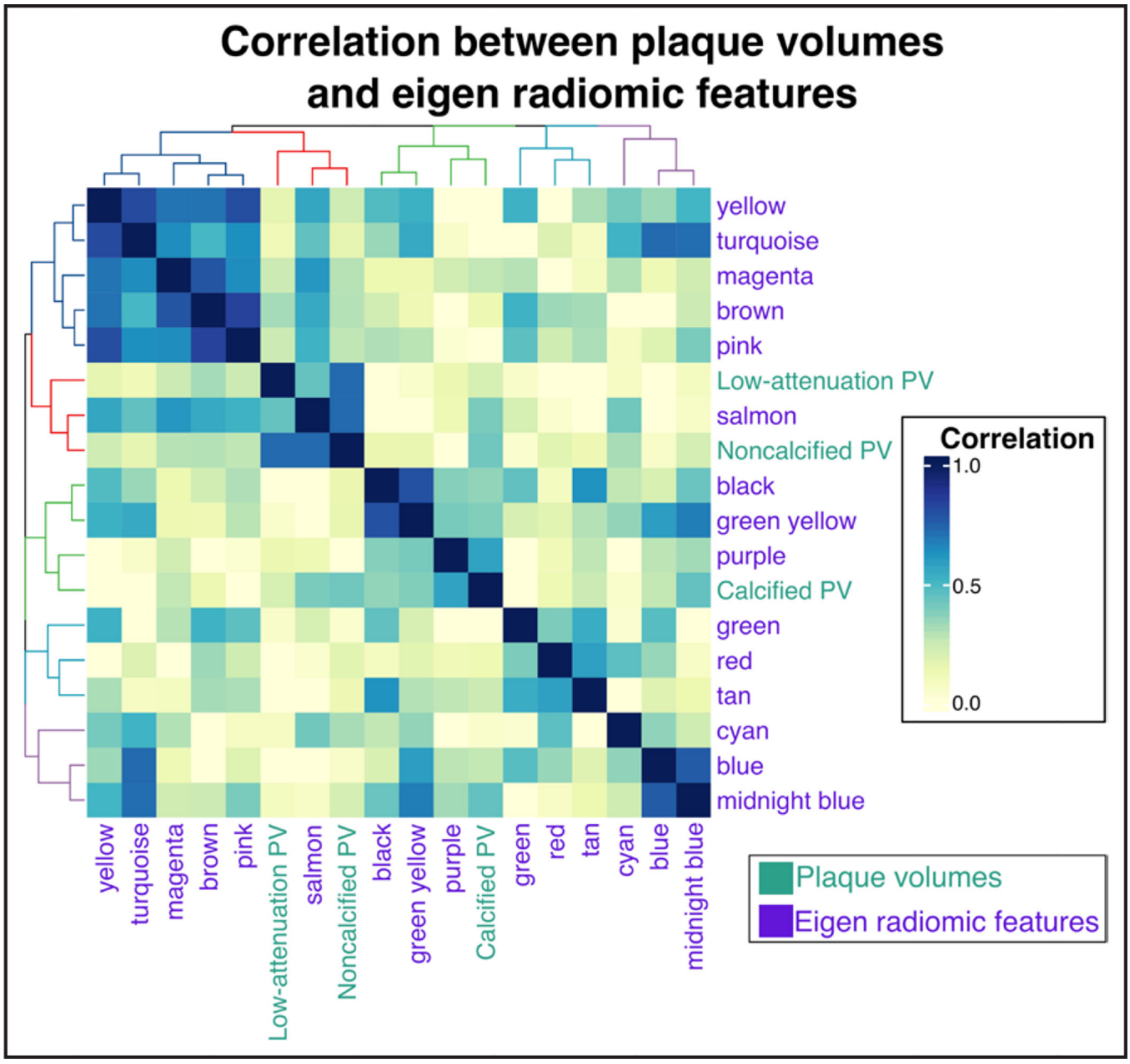

Figure 3. Association between plaque volumes and latent plaque morphological features.

Heatmap demonstrating the correlations between eigen radiomic features and coronary plaque volumes (PV) derived from quantitative plaque analysis.

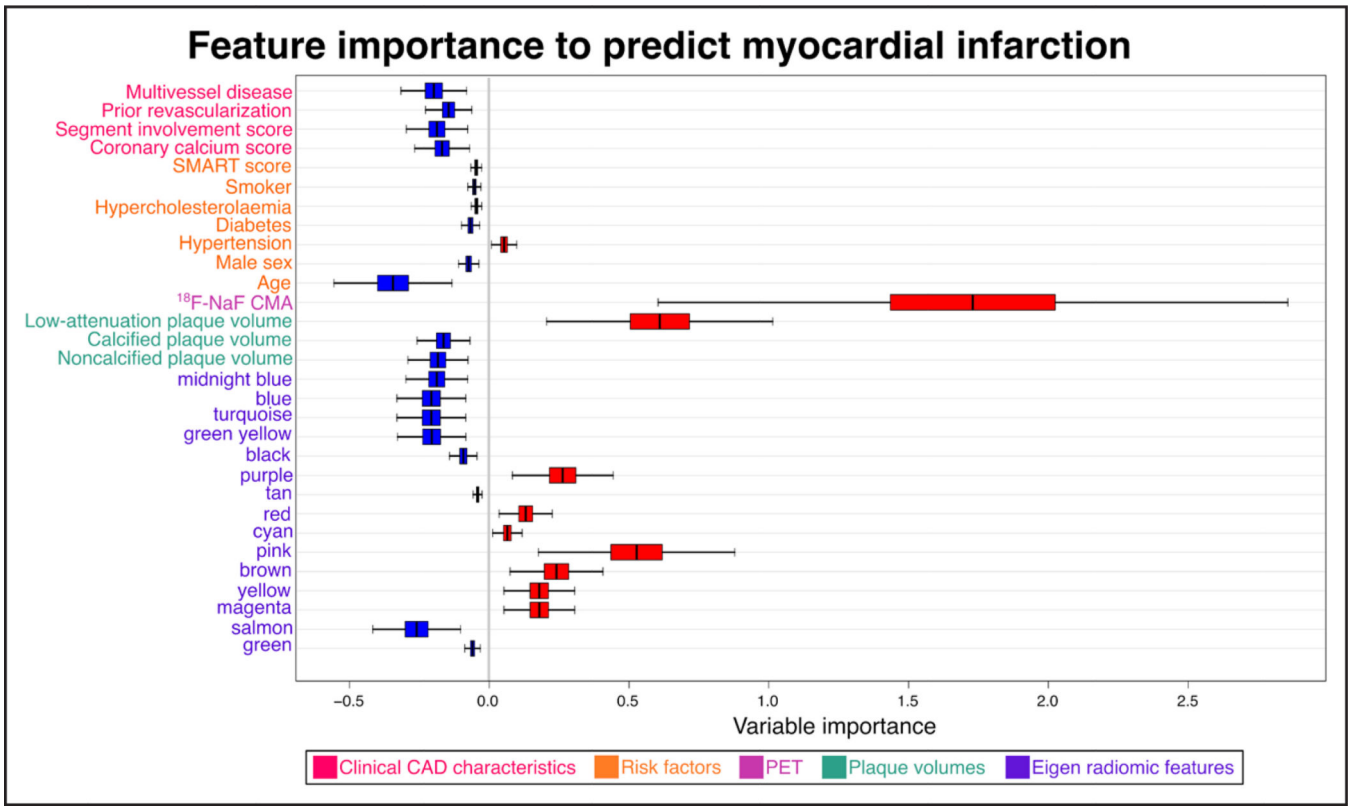

Figure 4. Predictors of myocardial infarction—variable importance according to the random forest machine learning model.

Variable importance and 95% CIs of clinical, positron emission tomography (PET), and coronary computed tomography angiography imaging parameters to predict myocardial infarction. Significant predictors are color-coded in red. ^{18}F-NaF CMA indicates ^{18}F-sodium fluoride coronary microcalcification activity; CAD, coronary artery disease; and SMART, Secondary Manifestations of Arterial Disease.

Table 1.

Baseline Clinical Characteristics

Category	Variable	Mean±SD/median[Q1–Q3]/n (%)
Baseline clinical characteristics	Age	65±9
	Men	216 (83%)
	Body mass index, kg/m^2	29 [26–32]
	Systolic blood pressure, mm Hg	139±17
	Diastolic blood pressure, mm Hg	77±12
Cardiovascular history	History of acute coronary syndrome	153 (59%)
	History of percutaneous coronary intervention	191 (73%)
	History of coronary artery bypass graft surgery	24 (9%)
Comorbidities/risk factors	Hypertension	153 (59%)
	Hyperlipidemia	235 (90%)
	Diabetes	54 (21%)
	Current smoking	47 (18%)
	Exsmoker	125 (48%)
	Atrial fibrillation	7 (3%)
	Peripheral vascular disease	14 (5%)
Medications *	Aspirin	238 (92%)
	Statin	231 (89%)
	Beta-blocker	173 (67%)
	Angiotensin-converting enzyme inhibitor or angiotensin receptor blocker	182 (70%)
	Insulin	4 (2%)
	Oral diabetic medications	42 (16%)
	Calcium blockers	56 (22%)
	Diuretics	66 (25%)
Biomarkers	Total cholesterol, mg/dL	4.1 [3.6–4.4]
	LDL cholesterol, mg/dL	2.0 [1.4–2.5]
	HDL cholesterol, mg/dL	1.2 [1.0–1.6]
	Triglycerides, mg/dL	1.5 [1.1–2.3]

Category	Variable	Mean±SD/median[Q1–Q3]/n (%)
Computed tomography— qualitative and noncontrast	Single vessel disease	78 (30%)
	Two vessel disease	101 (39%)
	Three vessel disease	81 (31%)
	Left main stem involvement	15 (6%)
	Coronary stent	197 (76%)
	Segment involvement score	6 [4–7]
	Segment involvement score >5	197 (76%)
	Coronary calcium score (AU)	294 [75–775]
	Coronary calcium score category	
	0–99 AU	76 (29%)
	100–399 AU	43 (17%)
	400–999 AU	83 (32%)
	>1000 AU	58 (22%)
Computed tomography— quantitive	Total plaque volume, mm^3	1174 [737–1787]
	Noncalcified plaque volume, mm^3	1100 [665–1574]
	Calcified plaque volume, mm^3	73 [25–141]
	Low-attenuation plaque volume, mm^3	86 [44–164]
	Total plaque burden, %	56 [47–64]
	Noncalcified plaque burden, %	51 [45–57]
	Calcified plaque burden, %	3 [1–7]
	Low-attenuation plaque burden, %	4 [3–7]
^{18}F-NaF PET	CMA	0.64 [0–2.53]
Outcome	Myocardial infarction	18 (7%)

^{18}F-NaF PET, ^{18}F-sodium fluoride positron emission tomography; AU, Agatston units; CMA, coronary microcalcification activity; HDL, high-density lipoprotein; and LDL, low-density lipoprotein.

*Medication at the time of ^{18}F-NaF PET imaging.

Table 2.

Clustered Radiomic Coronary Plaque Features and Coronary ^{18}F-NaF Uptake

	Univariate linear regression		Multivariate linear regression*	
Eigen radiomic feature	**β (95% CI)**	***P* value**	**β (95% CI)**	***P* value**
Green	0.02 (−0.03 to 0.08)	0.36	0.01 (−0.04 to 0.07)	0.64
Salmon	0.12 (0.06 to 0.18)	<0.001	0.03 (−0.04 to 0.11)	0.43
Magenta	0.13 (0.08 to 0.19)	<0.001	0.06 (−0.001 to 0.12)	0.053
Yellow	0.05 (−0.01 to 0.10)	0.07	0.02 (−0.04 to 0.08)	0.47
Brown	0.07 (0.02 to 0.12)	0.01	0.03 (−0.03 to 0.09)	0.40
Pink	0.07 (0.01 to 0.12)	0.02	0.04 (−0.01 to 0.10)	0.14
Cyan	0.01 (−0.03 to 0.05)	0.96	−0.02 (−0.08 to 0.04)	0.49
Red	0.02 (−0.03 to 0.07)	0.48	−0.01 (−0.06 to 0.05)	0.90
Tan	0.02 (−0.03 to 0.08)	0.39	−0.03 (−0.09 to 0.02)	0.22
Purple	0.24 (0.19 to 0.30)	<0.001	0.15 (0.08 to 0.22)	<0.001
Black	0.12 (0.07 to 0.17)	<0.001	0.04 (−0.02 to 0.09)	0.17
Green-yellow	0.17 (0.12 to 0.22)	<0.001	0.08 (0.03 to 0.14)	0.004
Turquoise	0.01 (−0.04 to 0.07)	0.51	0.02 (−0.04 to 0.07)	0.54
Blue	0.13 (0.08 to 0.18)	<0.001	0.07 (0.01 to 0.12)	0.014
Midnight blue	0.21 (0.15 to 0.26)	<0.001	0.12 (0.06 to 0.18)	<0.001

Univariable and multivariable linear regression analysis of radiomic features and an increase in ^{18}F-NaF CMA. ^{18}F-NaF indicates ^{18}F-sodium fluoride; and CMA, coronary microcalcification activity.

*Adjusted for calcified, noncalcified, and low-attenuation plaque volumes.

Table 3.

Clustered Radiomic Coronary Plaque Features and Coronary ^{18}F-NaF Uptake

	Univariate logistic regression		Multivariate logistic regression*	
Eigen radiomic feature	**Odds ratio (95% CI)**	***P* value**	**Odds ratio (95% CI)**	***P* value**
Green	1.16 (1.01 to 1.36)	0.04	1.15 (0.98 to 1.35)	0.08
Salmon	1.49 (1.29 to 1.71)	<0.001	1.42 (1.16 to 1.76)	<0.001
Magenta	1.88 (1.58 to 2.24)	<0.001	1.65 (1.37 to 1.99)	<0.001
Yellow	1.50 (1.28 to 1.77)	<0.001	1.46 (1.23 to 1.74)	<0.001
Brown	1.45 (1.26 to 1.68)	<0.001	1.39 (1.19 to 1.63)	<0.001
Pink	1.50 (1.30 to 1.73)	<0.001	1.48 (1.27 to 1.74)	<0.001
Cyan	0.01 (−0.03 to 0.05)	0.96	1.03 (0.88 to 1.20)	0.75
Red	1.03 (0.89 to 1.19)	0.67	0.98 (0.84 to 1.13)	0.76
Tan	0.98 (0.85 to 1.13)	0.78	0.85 (0.74 to 0.99)	0.04
Purple	1.76 (1.52 to 2.03)	<0.001	1.63 (1.37 to 1.95)	<0.001
Black	1.22 (1.05 to 1.40)	0.007	1.00 (0.86 to 1.17)	0.99
Green-yellow	1.46 (1.26 to 1.69)	<0.001	1.20 (1.02 to 1.41)	0.03
Turquoise	0.83 (0.71 to 0.96)	0.02	0.80 (0.68 to 0.94)	0.01
Blue	1.41 (1.21 to 1.65)	<0.001	1.21 (1.03 to 1.42)	0.02
Midnight blue	1.43 (1.25 to 1.64)	<0.001	1.76 (1.01 to 1.38)	0.04

Univariable and multivariable logistic regression analysis of radiomic features and ^{18}F-NaF CMA>0. ^{18}F-NaF indicates ^{18}F-sodium fluoride; and CMA, coronary microcalcification activity.

*Adjusted for calcified, noncalcified, and low-attenuation plaque volumes.

Table 4.

Clustered Radiomic Coronary Plaque Features and Clinical Risk Factors

	Univariate linear regression					
	Hypertension		Diabetes		Hypercholesterolemia	
Eigen radiomic feature	β (95% CI)	*P* value	β (95% CI)	*P* value	β (95% CI)	*P* value
Green	0.25 (−0.01 to 0.49)	0.051	0.09 (−0.20 to 0.38)	0.55	0.34 (−0.09 to 0.87)	0.19
Salmon	0.11 (−0.29 to 0.51)	0.40	0.45 (0.05 to 0.84)	0.01	0.19 (−0.10 to 0.48)	0.45
Magenta	−0.02 (−0.31 to 0.64)	0.88	0.39 (0.06 to 0.72)	0.01	0.13 (−0.16 to 0.42)	0.61
Yellow	0.12 (−0.29 to 0.41)	0.35	0.28 (−0.02 to 0.58)	0.08	0.35 (−0.05 to 0.75)	0.16
Brown	0.16 (−0.06 to 0.39)	0.20	0.34 (0.02 to 0.66)	0.03	0.21 (−0.13 to 0.55)	0.42
Pink	0.20 (−0.09 to 0.48)	0.25	0.27 (0.05 to 0.49)	0.09	0.13 (−0.21 to 0.47)	0.61
Cyan	−0.15 (−0.36 to 0.06)	0.26	−0.17 (−0.38 to 0.04)	0.28	0.28 (−0.10 to 0.66)	0.28
Red	−0.10 (−0.44 to 0.24)	0.45	−0.19 (−0.43 to 0.05)	0.23	−0.28 (−0.64 to 0.08)	0.27
Tan	−0.15 (−0.51 to 0.31)	0.78	−0.04 (−0.30 to 0.22)	0.82	−0.39 (−0.82 to 0.04)	0.13
Purple	−0.28 (−0.60 to 0.04)	0.24	0.24 (−0.03 to 0.51)	0.11	−0.32 (−0.72 to 0.08)	0.20
Black	−0.10 (−0.32 to 0.12)	0.44	0.06 (−0.20 to 0.32)	0.71	−0.33 (−0.79 to 0.13)	0.20
Green-yellow	−0.03 (−0.21 to 0.15)	0.84	0.18 (−0.03 to 0.39)	0.26	−0.29 (−0.73 to 0.15)	0.25
Turquoise	0.06 (−0.28 to 0.40)	0.64	0.06 (−0.22 to 0.34)	0.70	−0.24 (−0.60 to 0.12)	0.37
Blue	0.10 (−0.19 to 0.39)	0.41	0.28 (−0.01 to 0.57)	0.06	−0.17 (−0.55 to 0.21)	0.48
Midnight blue	0.07 (−0.18 to 0.32)	0.58	0.46 (0.06 to 0.86)	0.004	−0.24 (−0.65 to 0.17)	0.35

Univariable linear regression analysis of clinical risk factors and radiomic features.

Table 5.

Univariable and Multivariable Cox Proportional Hazard Models Adjusted for Plaque Volumes and ^{18}F-NaF Coronary Uptake

	Univariate Cox proportional hazard model		Multivariate Cox proportional hazards model*	
Eigen radiomic feature	**Hazard ratio (95% CI)**	***P* value**	**Hazard ratio (95% CI)**	***P* value**
Green	1.39 (1.0–1.94)	0.051	1.42 (0.94–2.18)	0.09
Salmon	1.42 (1.05–1.91)	0.02	1.46 (1.03–2.08)	0.03
Magenta	1.32 (0.88–1.97)	0.18	1.43 (0.88–2.30)	0.15
Yellow	1.60 (1.09–2.34)	0.02	1.62 (1.04–2.54)	0.02
Brown	1.44 (1.08–1.93)	0.01	1.49 (1.07–2.06)	0.01
Pink	1.33 (1.05–1.69)	0.02	1.50 (1.05–2.13)	0.02
Cyan	0.73 (0.51–1.03)	0.07	0.69 (0.40–1.07)	0.11
Red	0.67 (0.44–1.02)	0.06	0.68 (0.36–1.09)	0.12
Tan	0.66 (0.27–1.0)	0.051	0.74 (0.48–1.13)	0.16
Purple	0.52 (0.27–1.0)	0.052	0.46 (0.12–1.04)	0.08
Black	0.79 (0.47–1.33)	0.38	0.81 (0.50–1.32)	0.40
Green-yellow	1.03 (0.66–1.59)	0.90	1.01 (0.61–1.68)	0.96
Turquoise	0.62 (0.29–1.31)	0.21	0.72 (0.36–1.44)	0.34
Blue	1.19 (0.79–1.82)	0.40	1.22 (0.74–2.03)	0.44
Midnight blue	1.09 (0.75–1.59)	0.65	1.03 (0.64–1.65)	0.90

*Adjusted for calcified, noncalcified, low-attenuation plaque volumes, and ^{18}F-sodium fluoride coronary microcalcification activity.